Sky coverage assessment for the European ELT: a joint evaluation for MAORY/MICADO and HARMONI

Cédric Plantet[a],[*],[†] Benoît Neichel,[b],[†] Guido Agapito,[a] Lorenzo Busoni,[a] Carlos M. Correia,[c] Thierry Fusco,[b,d] Marco Bonaglia,[a] and Simone Esposito[a]

[a]INAF, Osservatorio Astrofisico di Arcetri, Firenze, Italy
[b]Aix Marseille University, CNRS, CNES, LAM, Marseille, France
[c]Space ODT - Optical Deblurring Technologies, Porto, Portugal
[d]ONERA, Chatillon, France

Abstract. The instruments developed for the upcoming Extremely Large Telescopes (ELTs) will need efficient adaptive optics (AO) systems to correct the effects of the atmospheric turbulence and allow imaging at the highest angular resolution. One of the most important requirements for ELT AO-assisted instruments will be to deliver diffraction-limited images in a significant part of the sky. For that, the instruments will be equipped with laser guide stars (LGSs) providing most of the information required by AO instruments. But even with LGSs, AO systems still require the use of natural guide stars (NGSs) to compensate for image motion (jitter) and some low order aberrations. These NGSs are eventually limiting the fraction of the sky that can be achieved by AO systems, the so-called sky coverage (SC). We first present the SC assessment methods used for high angular resolution monolithic optical and near-infrared integral field spectrograph (HARMONI) and multiconjugate adaptive optics relay/multi-AO imaging camera for deep observations (MAORY/MICADO), that are both instruments for the ELT of the European Southern Observatory (ESO). They are based on a semianalytical description of the main contributors in the AO error budget, allowing for a fast estimation of the residual jitter. As such, these methods are well suited for statistical estimation of the SC on multiple science fields and/or to efficiently explore the system parameter space. We then compute the SC of the two instruments in cosmological fields from the cosmic assembly near-IR deep extragalactic legacy survey catalog. The goal is to provide an insight on the possibilities given by two different types of tomographic AO systems, i.e., laser tomography AO with HARMONI and multiconjugate AO with MAORY, on the same telescope. In particular, we show that HARMONI and MAORY/ MICADO are complementary, meaning that the overall SC of ESO's ELT is much improved for applications common to both systems. © *The Authors. Published by SPIE under a Creative Commons Attribution 4.0 International License. Distribution or reproduction of this work in whole or in part requires full attribution of the original publication, including its DOI.* [DOI: 10.1117/1.JATIS.8.2.021509]

Keywords: adaptive optics; wavefront sensing; multiconjugate adaptive optics; laser tomography adaptive optics; extremely large telescope.

1 Introduction

The Extremely Large Telescope of the European Southern Observatory (ESO's ELT[1]) will have a theoretical resolution better than 15 milli-arcsec (mas) in K band, which will lead to observations of unprecedented quality. However, to reach this resolution in real conditions, it is necessary to compensate for the atmospheric turbulence effects on the incoming light with the help of an adaptive optics (AO) system. The AO system should be able to provide a satisfying performance in a significant portion of the sky, i.e., a good sky coverage (SC), to allow the observation of many objects and consequently studies that are statistically robust.

---

*Address all correspondence to Cédric Plantet, cedric.plantet@inaf.it

[†]Cofirst authors.

The three first-light instruments of ESO's ELT, i.e., MAORY/MICADO (multiconjugate adaptive optics relay/multi-AO imaging camera for deep observations),[2,3] HARMONI (high angular resolution monolithic optical and near-infrared integral field spectrograph),[4,5] and METIS (mid-infrared ELT imager and spectrograph),[6] will first implement single-conjugated AO (SCAO) corrections. In this case, the AO system is using a single natural guide star (NGS) and provides correction over a limited field of view (FoV) and SC. Indeed, this latter is limited by the fact that the SCAO system will typically require an NGS with a magnitude of $R < 14$ within 10 arcsec. [7–9] The associated SC (or the probability to find such a configuration) is then only about 1% of the whole sky.[10] To improve the SC, the ELTs will implement multilaser guide stars (LGSs), providing bright artificial sources at any place over the sky.[11] The use of multi-LGSs can then significantly improve the SC. But LGSs suffer from two major limitations, known as cone effect and tip–tilt (TT) indetermination.[12] The first one (cone effect) is simply due to the fact that the LGS is produced at a finite distance (the sodium layer at about 90 km above the telescope), hence the volume of turbulence its light crosses is conic, whereas it would be cylindrical for an NGS. This cone effect prevents the use of a single LGS for an ELT-size telescope and multiple LGSs (typically 6 to 8) are thus deployed, to pave the turbulent volume. This paving of the turbulence allows a tomographic reconstruction and the turbulent wavefront can then be corrected along the optical axis (laser tomography AO or LTAO),[5] with a single deformable mirror (DM) as in SCAO, or even on a wider FoV (multiconjugate AO or MCAO), with several DMs optically conjugated to different altitudes.[13,14] The second main limitation (TT indetermination) comes from the fact that the laser light passes through the exact same path on the way up and down.[15] Hence, the relative position of the LGS with respect to the background NGSs is unknown. As a first order, this means that the image position, or image jitter, cannot be compensated with a LGS. Therefore, all AO-LGS systems have to be complemented by the use of at least one NGS to control the fast image jitter induced by the atmospheric turbulence and other modes if needed. This or these NGSs can be faint, as only a few low order modes are to be evaluated, with typical foreseen limiting magnitude around $H = 19$ for ESO's ELT.[5] They may also be chosen in a technical field of a few arcminutes, resulting in a typical SC better than 50%.

At this point it is important to properly define the notion of SC. Indeed, to be meaningful, the SC has to be associated to a given performance.[16] This performance may be expressed in terms of residual jitter (e.g., in mas), in nanometers of wavefront error or in resulting Strehl ratio (SR), and the SC will be the fraction of the sky over which the AO system will be able to deliver this performance or better. It also important to emphasize that this performance will not be uniform across the sky but will follow the density distribution of the stars. To a first order, SC will be two orders of magnitude better nearby the galactic plane than at the galactic poles, where the star density becomes very small.[17] Another illustrative example concerns the cosmological fields, where a large fraction of extragalactic observations are done. In that sense, extragalactic studies are not homogeneously distributed across the sky, but mostly concentrated on a few specific fields, where multiwavelength observations are available. Those fields have generally been chosen to be located outside of the galactic plane to avoid contamination by dust, but also, in regions lacking bright stars to allow for long exposures without risk of science detectors saturation.[18] This is obviously perpendicular to the AO needs in terms of NGS requirements and biases the SC. But as these fields are of particular interest for the astronomical community, it is of importance to estimate the AO performance in these specific regions.

In this paper, we focus on the SC estimation of the two tomographic AO systems respectively providing a correction for HARMONI and MICADO. The first one is an LTAO system, called H-LTAO, and the second one, MAORY, is an MCAO system. We first present the SC assessment methods of the two instruments. These methods are very similar and are based on an analytical description of the jitter control, which allows for a fast estimation of the performance. This latter point is crucial in the design phases of instrument, as one wants to explore a wide system and atmospheric parameter space. This also allows for statistical studies of SC, computing the performance for hundreds of scientific fields. Taking advantage of this computational capability, we compute the SC of H-LTAO and MAORY in synthetic fields from the Besancon galaxy model[19] and in known cosmological fields from the cosmic assembly near-IR deep extragalactic legacy survey (CANDELS) catalog.[20,21] This comparison gives an insight on the possibilities provided

by each instrument. In particular, we show that they have a complementary SC, meaning that the overall SC is greatly improved for applications that are common to both systems.

The assumptions and simulation inputs are presented in Sec. 2, the semianalytical methods are presented in Sec. 3, and the applications on synthetic fields and on cosmological fields are presented in Sec. 4. Finally, we discuss the results and conclude in Secs. 5 and 6.

2 Assumptions and Tools

In this section, we list the tools and the default assumptions used throughout the study.

2.1 *Error Budget Approach*

To assess the performance in a given configuration, one needs either to perform a full end-to-end (E2E) simulation and/or use analytical/semianalytical tools. In this latter approach, the fundamental assumption is that all the contributors to the final performance are fully uncorrelated and can be estimated independently. This is an error budget approach, where the final performance is the result (the sum) of independent contributors. This approach is convenient as typically each term of the error budget can be estimated by analytical formulae, which makes the whole process extremely fast when compared with full E2E simulations. Of course, the performance assessment will not be as accurate as with E2E simulations, but it allows to narrow the parameter space efficiently. In this study, we will follow this error budget approach, with the first assumption that all the high-order (HO) part of the error budget (related to the LGSs measurements) are evaluated independently. We thus only focus on the low-order (LO) part of the error budget and mostly on the residual jitter estimation.

2.2 *Atmospheric Parameters*

The studies for both systems have been done using the same C_n^2 profiles that were provided by ESO.[22] Most of the SC study relies on the median profile that has 35 layers ranging from 30 to 26,500 m, with 70% of the turbulence below 600 m (approximate conjugation altitude of M4 and the DM of ESO's ELT). The median seeing is 0.644 in. (defined at zenith and at 500 nm) and the outer scale is 25 m. The other C_n^2 profiles correspond to the four quartiles. They are very similar to the median profile in terms of energy distribution, but they have different seeings. In the following, we also assume that all the performances are estimated for a zenith angle of 30 deg.

2.3 *System Parameters*

Being both tomographic AO systems, MAORY and H-LTAO have some similarities. However, they still are two different types of system, with different requirements: H-LTAO should provide a good correction only on axis, while MAORY should provide a wide-field correction. Another main difference is the patrol field of the NGS wavefront sensors (WFS), a.k.a. technical FoV: H-LTAO can pick its NGS close to the axis, while MAORY must make use of NGSs far off axis to avoid vignetting the scientific FoV. However, MAORY's NGSs can get a bit closer to the axis when MICADO uses its small FoV, as the vignetting area decreases. The configuration for each system is listed in Table 1. The optimized FoV as stated in the table is the so-called FoV of interest in Ref. 14.

The NGS WFS for both MAORY and H-LTAO will have 2×2 subapertures to be able to sense the focus at lower frequency and correct the sodium layer altitude variations on the LGS WFSs.[23] In the following, we consider these sensors as TT sensors only (with the appropriate noise due to their subaperture geometry), and we add a fixed amount of focus in the error budget, that is, the residual of the sodium altitude variations.

For H-LTAO, given that the SR on the NGSs might be low because of the off-axis distance, a solution to increase the signal-to-noise ratio on the NGS WFSs has been considered in the SC study. This solution consists in adding an open-loop DM (OLDM) in the path of the NGS WFS. This so-called dual AO[24] would correct up to a few hundred wavefront modes to increase the sensitivity of the NGS WFSs. This solution is not required for MAORY, as the multiple DMs in the path can compensate for the atmosphere in a wider FoV.

Table 1 System configurations for H-LTAO and MAORY. For MAORY, the DM configuration is presented as baseline/upgrade. The inner border radius of MAORY's technical FoV takes into account the potential vignetting of the scientific FoV by the pick-off mirrors. The LGSs are uniformly distributed on a circle of the specified radius.

Parameter	MAORY	H-LTAO
Technical FoV (radius)	Annulus: 49" to 80" (24" to 80" for small MICADO FoV)	60"
# DMs	Baseline: 2 Upgrade: 3	1
DM altitudes	Baseline: 621 m (M4), 17.6 km Upgrade: 621 m (M4), 7.4 km, 17.6 km	621 m (M4)
DM pitches	Baseline: 0.5 m, 1.5 m (970 modes) Upgrade: 0.5 m, 1 m (1690 modes), 1.5 m (970 modes)	0.5 m
# LGSs	6	6
# NGSs	Up to 3	1
LGS asterism radius	45"	34"
# modes on the NGSs	2 (TT)	2 (TT)
# subapertures (NGS sensors)	2×2	2×2
Optimized FoV radius	30"	0" (on axis only)

2.4 Windshake

The secondary mirror (M2) of ESO's ELT will be close to the dome aperture and thus undergo a rather strong wind in some cases, causing high-amplitude vibrations. ESO provided the first-light instruments consortia with a data package,[25] in which one can find a 300-s time series of the wavefront TT due to such a windshake. This time series corresponds to a worst-case scenario: external wind 10 m/s (scenario), wind in the dome 8 m/s (scenario), frontal wind with respect to the telescope (worst condition), telescope zenith distance pointing 45 deg (worst condition for frontal wind), and wind screen deployed up not to vignette the telescope aperture (normal operating setup). The temporal power spectral densities (PSD) of the TT corresponding to the time series are plotted in Fig. 1. Depending on the telescope orientation with respect to the wind direction, one axis can be more excited than the other, which is the case in this scenario where the tilt gathers more energy than the tip. The TT from the windshake is isoplanatic (according to ESO studies), so one NGS is sufficient to sense it.
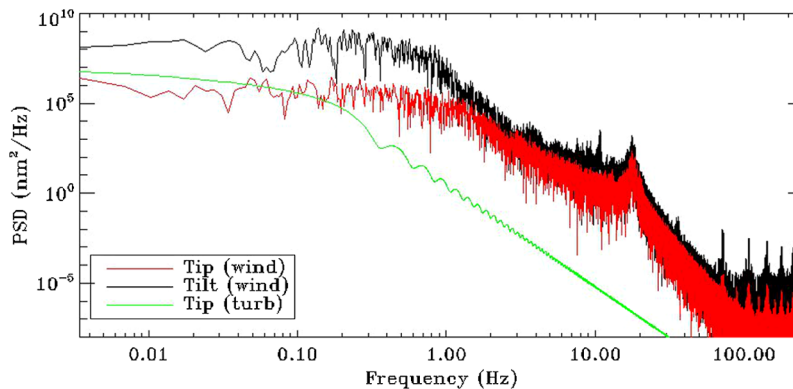

Fig. 1 Temporal PSDs of the TT due to the windshake on M2, compared with the turbulence PSD. The PSDs are computed from the time series using a Hanning window.

Several strategies can be adopted for the correction:

- Telescope only: The windshake is corrected using the telescope probes only. The residual jitter is then independent from the NGS asterism used by the AO system.
- Sequential: The windshake is only corrected by one of the NGS sensors of the AO system.
- Cascaded: The windshake is mostly corrected by the telescope, then the residual is corrected by the NGS sensors of the AO system.

For H-LTAO, the two last approaches are considered, while only the sequential control has been studied for MAORY.

2.5 Stars Statistics

The SC analysis requires a list of stars with their respective positions and magnitudes. This list can either be directly taken from a real star catalog or generated from a galaxy model. In the latter case, stars are randomly placed with a uniform distribution in the FoV corresponding to the query. In the following, we show results both with the CANDELS catalog[20,21] and with the Besancon galaxy model.[19]

3 Sky Coverage Assessment Method

The approaches of MAORY and H-LTAO to assess the SC are very similar, as they follow the same steps. We describe these steps hereafter, specifying the differences between the two systems.

3.1 Asterism Selection

At this point, we have a list of star positions and magnitudes in a wide FoV, and we generate a series of pointing coordinates with a uniform distribution. For each pointing, in the case of MAORY, we register all asterisms that are geometrically valid with respect to the technical FoV size, the pick-off mirror size, and the overlap between sensors (Fig. 2). If no three-star asterism is found, we look for two-star asterisms. Again, if we find no valid asterism, we select each star individually. The reason why we do not consider all asterisms (one NGS, two NGSs, or
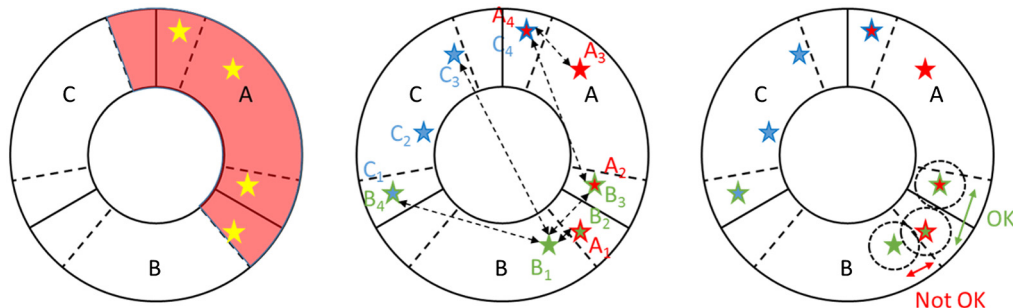

Fig. 2 Method to detect a valid configuration in the case of MAORY. The sensors' dedicated working areas are delimited by the solid lines, while the dashed lines indicate the possible extension of these areas. Between two dashed lines, we thus have an overlap zone between two sensors. Steps are, from left to right: (1) register all the stars under the limiting magnitude reachable by each sensor (remove those too close to the center to avoid vignetting). In this figure, we show the example for WFS A (the same is done for WFSs B and C). The red color shows the total area eventually reachable by the WFS A. Here, the star symbols are the potential NGSs for this sensor. (2) Compute distances between the registered stars. Here, the stars are color-coded as a function of which sensor can reach it (filling color = dedicated zone, contour color = overlap zone): red for WFS A, green for WFS B, and blue for WFS C. They are also named accordingly as indicated in the figure (a star reachable by two sensors will have two names). (3) Check the combinations that avoid collisions of the pick-off mirrors. For example, B2/A1 cannot be selected together with B1, but it can be selected together with B3.

three NGSs) is purely computational. In the case of H-LTAO, we use only one NGS and there are no zonal constraints, we thus compute the performance for each individual NGS within the technical FoV.

3.2 *Performance Computation*

The final performance is computed from these different terms:

- High orders: residuals from the LGS sensing.
- Low orders: residuals from the NGS sensing.
- Additional error: constant residual from various sources (non-AO-correctable). This includes, but is not limited to, wavefront errors due to noncommon path aberrations, misalignment, and manufacturing.

The LO residuals are themselves separated in three parts: windshake, anisoplanatism/tomography, and noise propagation. We consider the temporal error from the low orders negligible with respect to the rest of the error budget.

3.2.1 *High orders*

For MAORY, the HO residuals are derived from E2E simulations, with an equilateral triangle of bright NGSs ($H = 10$) at 55". We verified that the HO residuals variation with the NGS asterism is negligible. We add a fixed amount of 190 nm, corresponding to non-AO-correctable errors or other isoplanatic residuals, to these E2E residuals and we get the following HO residuals for the respective distances 0", 15", 25", and 30":

- M4 + 1 post-focal DM (PFDM): 302, 304, 313, and 324 nm.
- M4 + 2 PFDMs: 298, 302, 308, and 314 nm.

For H-LTAO, the HO residuals are also derived from E2E simulations, including all the atmospheric and telescope effects, but using a bright on-axis NGS. The performance is only to be estimated on-axis and provides an error budget of 270 nm.

3.2.2 *Windshake*

As stated in Sec. 2.4, 2 different strategies can be considered: sequential or cascaded.

For the sequential control, the windshake is sensed on the brightest available NGS. Indeed, with the AO system alone, a high loop frequency is needed to be able to correct the high-amplitude TT induced by the windshake. The residual TT is then computed by applying a temporal filter to the windshake PSD. This filter is

- H-LTAO: a linear quadratic Gaussian + second-order auto regressive (AR2) command. The filter is optimized for the control update based on the NGS magnitude.
- MAORY: a filter of order 2, with its poles, zeros, and gain optimized with respect to the NGS magnitude and SR, i.e., with respect to the noise level.

The residual in mean square error (MSE) is then

$$\text{MSE} = \int_0^\infty [|\text{RTF}|^2 \text{PSD}_{\text{wind}} + |\text{NTF}|^2 \text{PSD}_{\text{noise}}] \mathrm{d}f, \tag{1}$$

where RTF is the rejection transfer function and NTF is the noise transfer function corresponding to the temporal filter. The computation of the noise level for H-LTAO is described in Sec. 3.2.4. For MAORY, the noise level is computed from a Gaussian point spread function (PSF) model, with the flux scaled with the SR, and from the weighting maps used for local slope computation. Note that this method, which should lead to results similar to the ones of H-LTAO, is only used

for the windshake residual computation, and the noise considered for the tomographic correction of atmospheric TT is the one described in Sec. 3.2.4.

The cascaded mode (only considered for H-LTAO) is a mix of the telescope and instrument control. The windshake PSD becomes a residual TT PSD, but an arbitrary level of jitter is still added to account for the errors related to the telescope probes. In this case, the command is optimized in frequency according to the noise level, hence according to the NGS magnitude and SR.

3.2.3 *Pure tomographic error*

The pure tomographic error is due to the asterism geometry. For MAORY, it is computed using the method detailed in Appendix A. For H-LTAO, only one NGS is used, so the tomographic error simply is the anisoplanatism error that can be retrieved from the same formulas.

3.2.4 *Noise propagation*

For MAORY, to have a measurement noise level as a function of a star's distance and magnitude, we perform a series of E2E simulations changing only the NGS asterism, and we repeat it for five atmosphere occurrences. The NGSs are always on an equilateral triangle and all have the same magnitude. The loop frequency is adapted to the magnitude. In the end, we have a total of 5×18 simulations for each considered configuration, using the following distances and magnitudes:

- Distance: 30", 55", 65", and 80".
- H magnitude: 10, 17, 18, 19, 20, 21.

For each of these simulations, the residual in the directions of the NGSs is averaged, so that we have a residual per distance and magnitude. Then, for each star of each asterism considered in the SC computation, we interpolate these residuals at the star's distance and magnitude and consider the obtained value as the noise level on that star. This means that we also include the aliasing error and the temporal error in the noise term. It does not have a significant impact on the final residual, since the aliasing error propagates the same way as the noise in the loop, and we can consider the temporal error to be negligible with respect to the other terms (it amounts to about 0.4 mas at the faint end). The noise term is then propagated through the tomographic reconstructor as described in Appendix A. Note that this computation remains the same for both MICADO's large and small FoVs. The only difference between the two configurations is in the asterism selection.

In the case of H-LTAO, the noise on the Shack–Hartmann (SH) slopes has been computed based on E2E simulations, from which general abacuses are derived. The basic scheme of the E2E simulation is described by Fig. 3 and follows five steps: (1) computation of short exposure SH PSFs for various LTAO configurations and for various positions in the FoV. This computation includes the full telescope pupil parameters (central obstruction value for instance) and SH configurations (number of subaperture, wavelength), (2) known tilts are then added to each PSF, (3) additional defects (atmospheric dispersion corrector residuals, static aberrations, and object size) can also be added, as well as various types of noise (photon, background, and read-out-noise), (4) centroiding is measured on those SH images, with several possible techniques, and (5) the tilt is reconstructed from the measurement, leading to the residual tilt error and variance.

This procedure is repeated for different positions in the field, hence different level of AO correction. As an illustration, Fig. 4 shows the one axis tilt error variance for different number of photons and different positions of the NGS in the field. As a reference, 200 photons per frame correspond to a magnitude $H = 18.5$. This plots are then fitted with analytical equations (see next equations), which will eventually be used in the SC analysis.

To account for the residual phase (and thus the spread of photons outside the diffraction core), the analytical variance equations (as defined in Ref. 26) have to be modified as follows, for the photon noise and the read-out noise (RON):
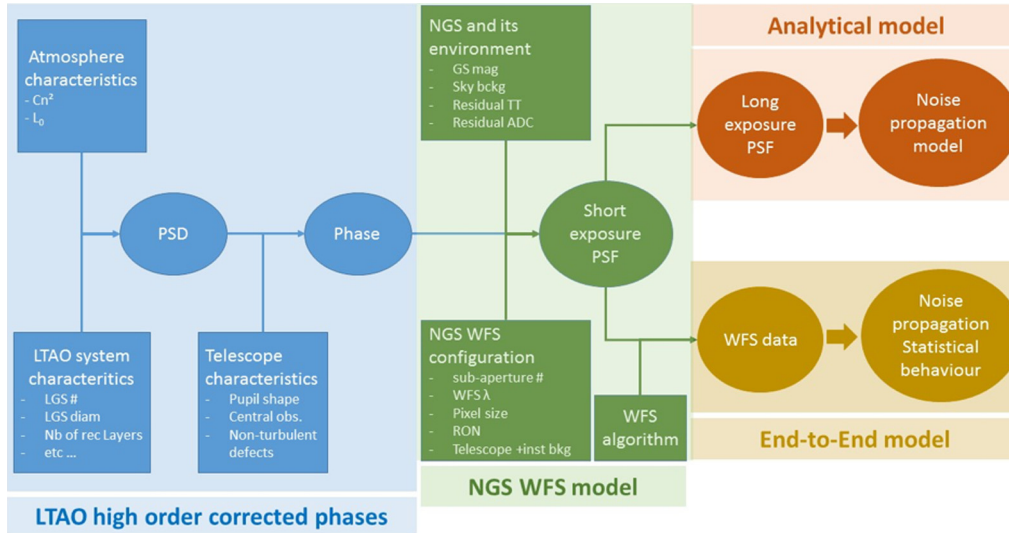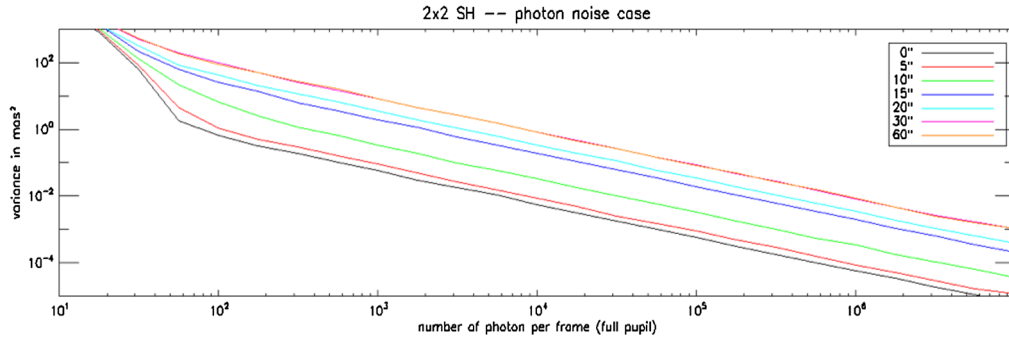
Fig. 3 Global scheme of the E2E TT noise estimation.

Fig. 4 Example of noise computed for a 2×2 SHWFS, for different level of fluxes, and different position of the NGS in the field, in the case of an LTAO correction without OLDM.

$$\sigma^2_{\text{ph,sspup,SR}} = \frac{1}{SR\, 2\, \ln(2) N_{\text{ph}}} \frac{N_T^2}{N_D^2} \left(\frac{N_T^2 + N_W^2}{2N_T^2 + N_W^2} \right)^2, \tag{2}$$

$$\sigma^2_{\text{ron,sspup,SR}} = \frac{\pi}{SR^2\, 32\, \ln(2)} \frac{ron^2}{N_{\text{ph}}^2} \left(\frac{N_T^2 + N_W^2}{N_D^2} \right)^2, \tag{3}$$

where N_{ph} is the number of photons, N_D is the full width at half maximum (FWHM) of the diffraction-limited PSF, N_T is the FWHM of the actual PSF, and N_W is the FWHM of the weighting function used for the weighted center of gravity.

When the PSF is no more diffraction limited, the FWHM (N_T) becomes the major contributor of the variance and the noise variances become again the classical ones:

$$\sigma^2_{\text{ph,sspup,FWHM}} = \frac{1}{2\, \ln(2) N_{\text{ph}}} \frac{N_T^2}{N_D^2} \left(\frac{N_T^2 + N_W^2}{2N_T^2 + N_W^2} \right)^2, \tag{4}$$

$$\sigma^2_{\text{ron,sspup,FWHM}} = \frac{\pi}{32\, \ln(2)} \frac{ron^2}{N_{\text{ph}}^2} \left(\frac{N_T^2 + N_W^2}{N_D^2} \right)^2. \tag{5}$$

In practice, we will use a combination of both analytic expressions to account for both regimes. This is done using the following ad-hoc expression:
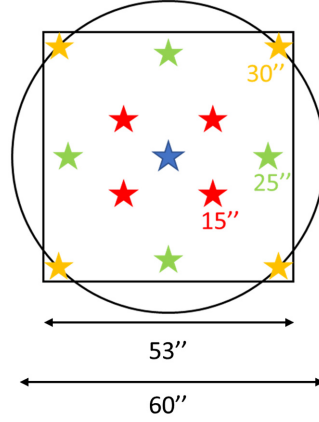
Fig. 5 Directions used for the jitter/SR computation in the FoV of 60" diameter. The square of side 53" corresponds to the large MICADO FoV. The stars are distributed as follows: one star on axis, four stars at 15", four stars at 25", and four stars at 30". When the small MICADO FoV is considered (20×20"), we average from one star on axis and four stars at 10" (placed in the same manner as the four stars at 15").

$$\sigma_{\text{tot}}^2 = \left(\frac{N_D}{N_T}\right)^2 \sigma_{\text{SR}}^2 + \left(1 - \left(\frac{N_D}{N_T}\right)^2\right)\sigma_{\text{FWHM}}^2. \tag{6}$$

In the SC study described below, the analytical laws will be used, which will allow us to quickly estimate the measurement noise for different NGS magnitude and position in FoV, as well for different configurations (central wavelength, number of subapertures, RON, elongation due to atmospheric dispersion corrector residual).

A numerical validation of the noise models presented in this section is shown in Appendix C.

3.3 *Sky Coverage Computation*

At this point, we are able to compute the jitter/SR for any direction in the scientific FoV and thus compute the SC.

For each pointing, we compute the LO residuals in the scientific FoV with all the possible asterisms and we register the lowest residual. For H-LTAO, we only need to compute the residual on axis, while for MAORY, the selection of the best asterism is based on the average LO residual in the FoV (using the directions shown in Fig. 5). We then add the HO residuals given in Sec. 3.2.1 to calculate the SR. Finally, we get the SC as the ratio between the number of fields giving an SR (jitter) greater (less) or equal to a given value and the total number of fields:

$$\text{SC}(x) = \frac{\sum_i P_i(\text{SR} \geq x)}{N_{\text{fields}}} \quad \text{or} \quad \text{SC}(x) = \frac{\sum_i P_i(\text{jitter} \leq x)}{N_{\text{fields}}}, \tag{7}$$

with $P_i(\text{SR} \geq x) = 1$ ($P_i(\text{jitter} \leq x) = 1$) if the i'th field has an asterism giving an SR (jitter) greater (less) than x and $P_i(\text{SR} \geq x) = 0$ ($P_i(\text{jitter} \leq x) = 0$) otherwise.

4 Sky Coverage Examples

4.1 *Synthetic Star Fields*

We first show an example of SC computation with the Besancon galaxy model for two regions of the sky: 1×1 deg at the following galactic coordinates: $l = 90$ deg, $b = -30$ deg and $l = 90$ deg, $b = -60$ deg. The results are plotted in Figs. 6 and 7 and the main numbers are reported in Tables 2 and 3. Here, we see the effect of the star density decreasing when going further from the galactic plane: lower jitter, or higher SR, can be obtained in all cases at $b = -30$ deg with respect to $b = -60$ deg.
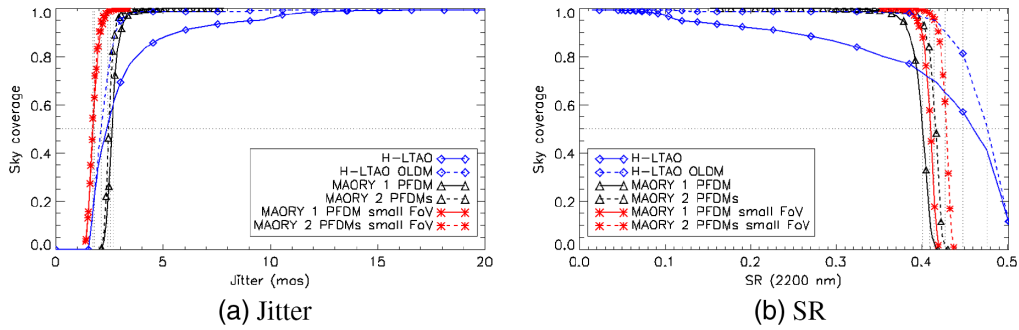
(a) Jitter　　　　　　　　(b) SR

Fig. 6 SC with H-LTAO or with MAORY at $l = 90$ deg, $b = -30$ deg. The jitter/SR is on axis for H-LTAO and averaged on a 1 arcmin diameter FoV (large FoV) or on a 20" diameter FoV (small FoV) for MAORY.
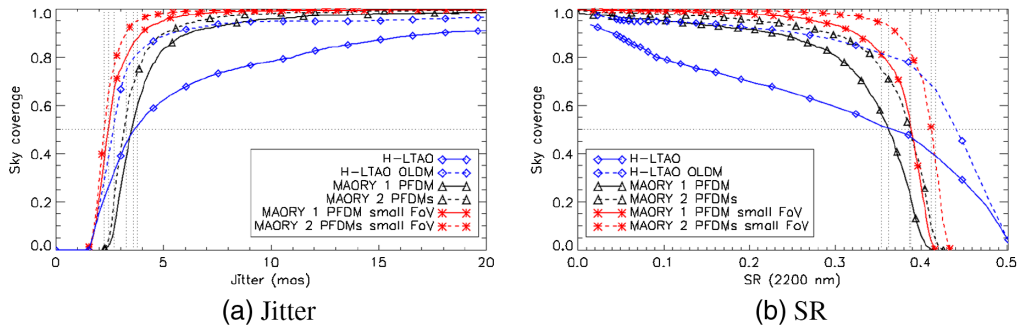

(a) Jitter　　　　　　　　(b) SR

Fig. 7 SC with H-LTAO or with MAORY at $l = 90$ deg, $b = -60$ deg. The jitter/SR is on axis for H-LTAO and averaged on a 1 arcmin diameter FoV (large FoV) or on a 20" diameter FoV (small FoV) for MAORY.

Table 2 Jitter/SR reached by the considered systems for different levels of SC at $l = 90$ deg, $b = -30$ deg.

Instrument/configuration	Jitter (mas)			SR (2200 nm)		
	25% SC	50% SC	75% SC	25% SC	50% SC	75% SC
H-LTAO	2	2.4	3.3	0.48	0.45	0.38
H-LTAO OLDM	1.8	2.1	2.6	0.48	0.48	0.45
MAORY 1 PFDM	2.4	2.6	2.8	0.41	0.4	0.39
MAORY 2 PFDMs	2.4	2.5	2.6	0.42	0.41	0.41
MAORY 1 PFDM small FoV	1.6	1.8	2	0.45	0.45	0.44
MAORY 2 PFDMs small FoV	1.6	1.7	1.9	0.46	0.45	0.45

4.2 *Application for Real Cosmological Fields*

We now apply the SC computation to cosmological fields that are taken from the CANDELS catalogs.[20] The five specific fields are shown in Fig. 8, with namely COSMOS, UDS, EGS, GOODS-S, and GOODS-N. (Note that GOODS-N and EGS will not be observable from ESO's ELT location. We still keep it for the SC analysis as it provides a representative example

Table 3 Jitter/SR reached by the considered systems for different levels of SC at $l = 90°$, $b = -60°$.

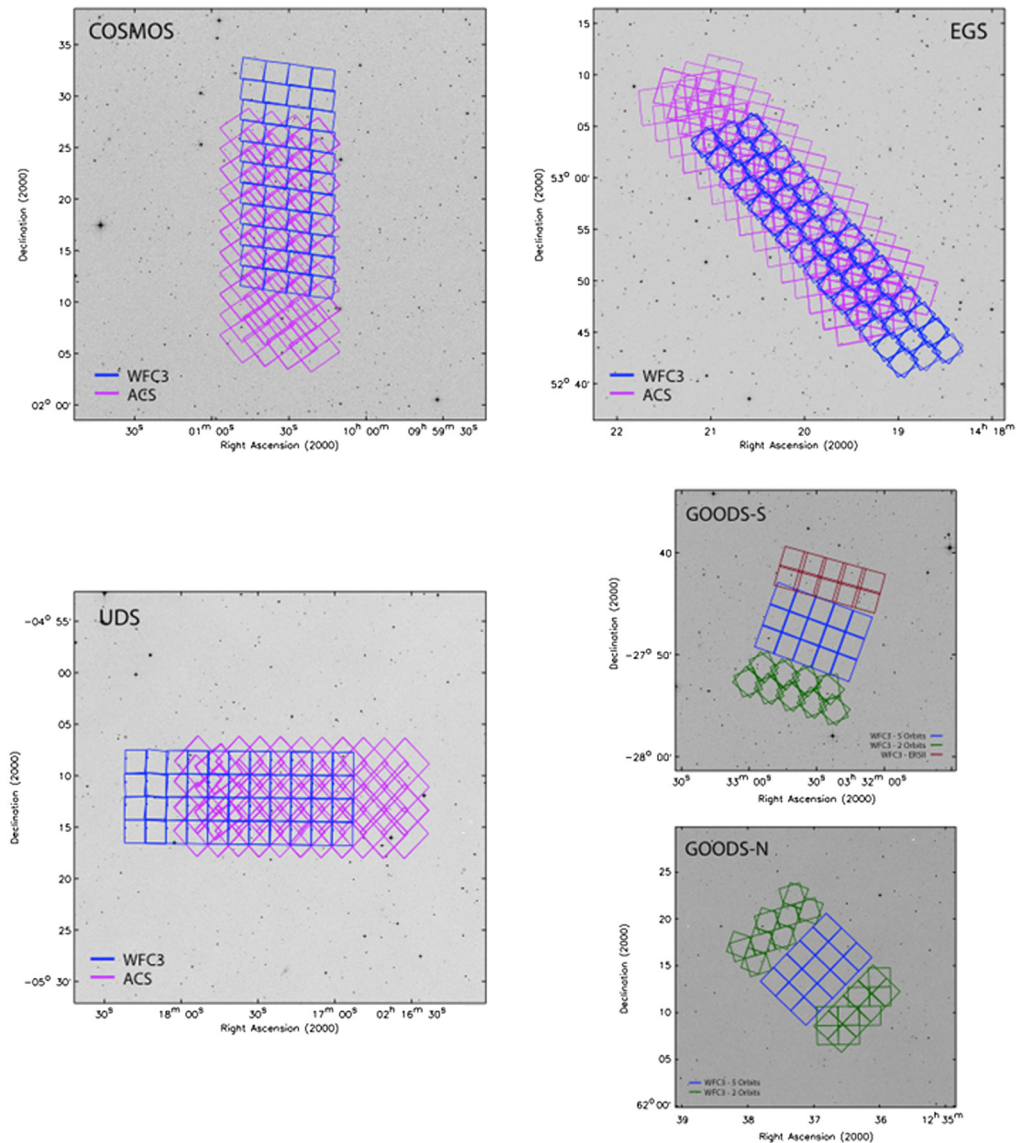| Instrument/configuration	Jitter (mas)			SR (2200 nm)		
	25% SC	50% SC	75% SC	25% SC	50% SC	75% SC
H-LTAO	2.4	3.8	8.3	0.45	0.35	0.14
H-LTAO OLDM	2.3	2.7	3.3	0.45	0.42	0.38
MAORY 1 PFDM	3	3.6	4.4	0.38	0.36	0.32
MAORY 2 PFDMs	2.8	3.3	3.9	0.4	0.39	0.35
MAORY 1 PFDM small FoV	2.1	2.4	3	0.43	0.42	0.4
MAORY 2 PFDMs small FoV	2	2.2	2.7	0.44	0.44	0.42

Fig. 8 Cosmological fields considered in this section. Taken from Ref. [20].

Table 4 Location, area and depth of the five cosmological fields used in the SC estimation for MAORY and HARMONI.

Field name	RA	DEC	Area	# of stars with H(Vega) < 21
GOODS-S	03h32m30s	−27°48′20″	~160 arcmin²	620
GOODS-N	12h36m55s	+62°14′15″	~160 arcmin²	240
UDS	02h17m49s	−05°12′02″	~204 arcmin²	321
COSMOS	10h00m28s	+02°12′21″	~204 arcmin²	474
EGS	14h17m00s	+52°30′00″	~205 arcmin²	348

of cosmological fields.) Table 4 summarizes some of the important characteristics of these fields for our present study.

These fields have been observed deeply and at multiple wavelengths with the Hubble Space Telescope as well as many other instruments. As such, they are privileged fields for extra-galactic studies and will likely be observed extensively with ESO's ELT. However, the fields considered here correspond to regions where bright NGSs are few, as they were chosen to facilitate the imaging of extragalactic objects. Of course, this is at the opposite of what the AO system requires to give an optimal performance. Therefore, evaluating the performance of the AO-assisted ELT instruments on these specific fields is or particular importance. These fields are also of interest as the catalogs available are complete down to $H < 26$ (Vega), which is five magnitudes deeper than what is required by the AO systems. All the technical details about these fields can be found in Ref. 20, in the following we only made use of the publicly available H-band catalogs.

Figures 9–18 show the evaluated jitter and SR maps for these fields, and the statistics of the jitter and SR for each field are given in Figs. 19–23. The main numbers of these statistics are reported in Tables 5–9. Note that we also consider the case in which the MICADO FoV is smaller
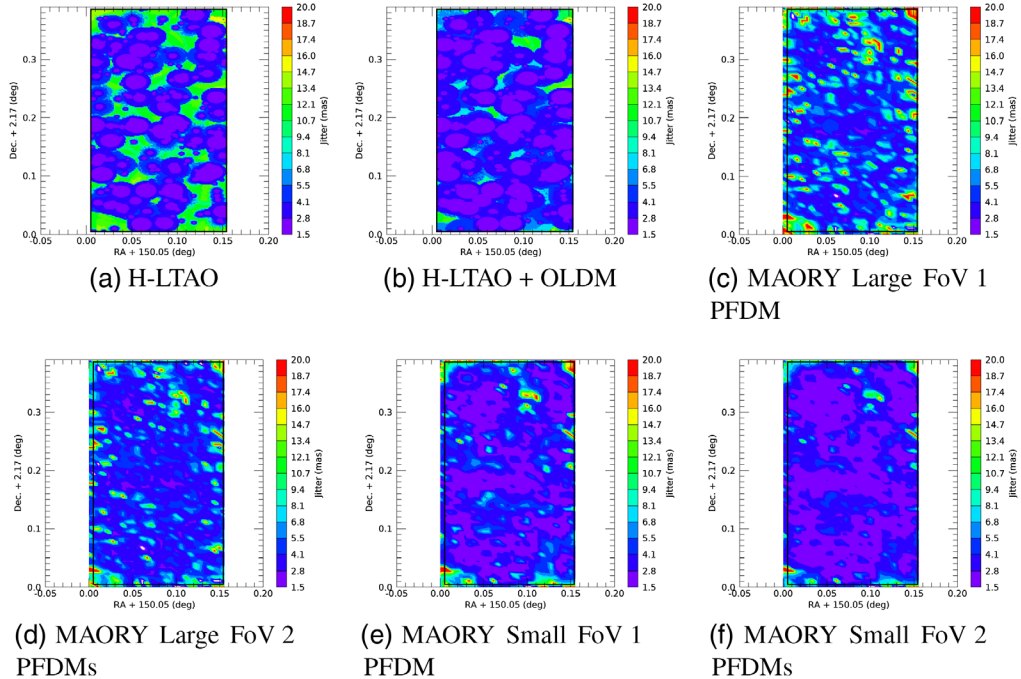

(a) H-LTAO

(b) H-LTAO + OLDM

(c) MAORY Large FoV 1 PFDM

(d) MAORY Large FoV 2 PFDMs

(e) MAORY Small FoV 1 PFDM

(f) MAORY Small FoV 2 PFDMs

Fig. 9 Jitter with H-LTAO (on axis) or with MAORY (averaged on the scientific FoV) for the COSMOS field. The jitter is limited to 20 mas for a better display. The black lines indicate the area used for the SC computation.
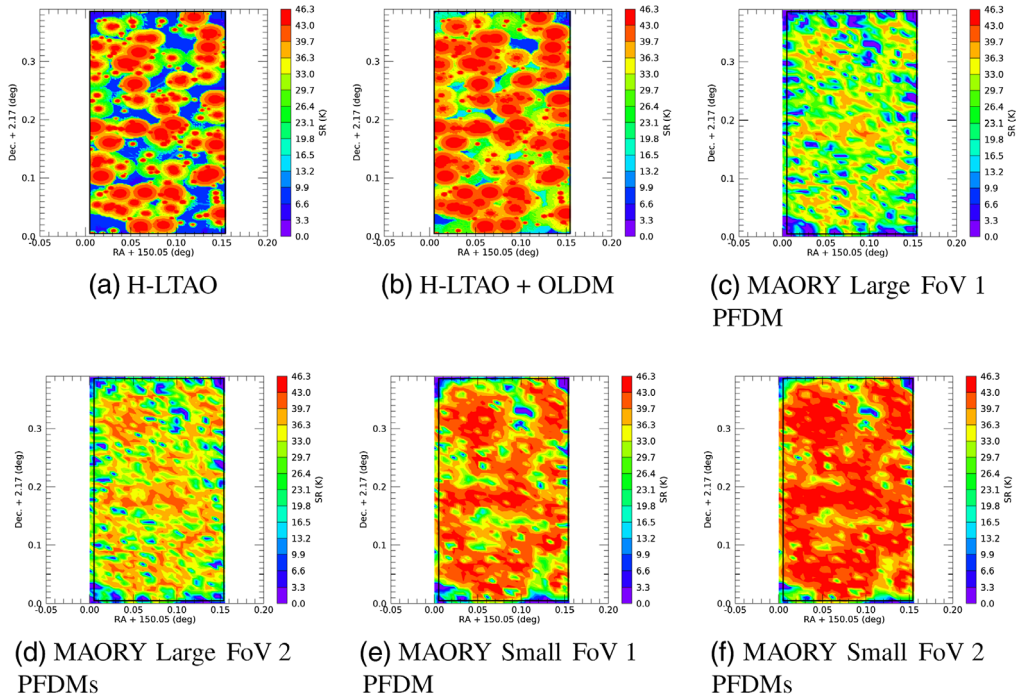
(a) H-LTAO

(b) H-LTAO + OLDM

(c) MAORY Large FoV 1 PFDM

(d) MAORY Large FoV 2 PFDMs

(e) MAORY Small FoV 1 PFDM

(f) MAORY Small FoV 2 PFDMs

Fig. 10 SR in K band with H-LTAO (on axis) or with MAORY (averaged on the scientific FoV) for the COSMOS field. The black lines indicate the area used for the SC computation.
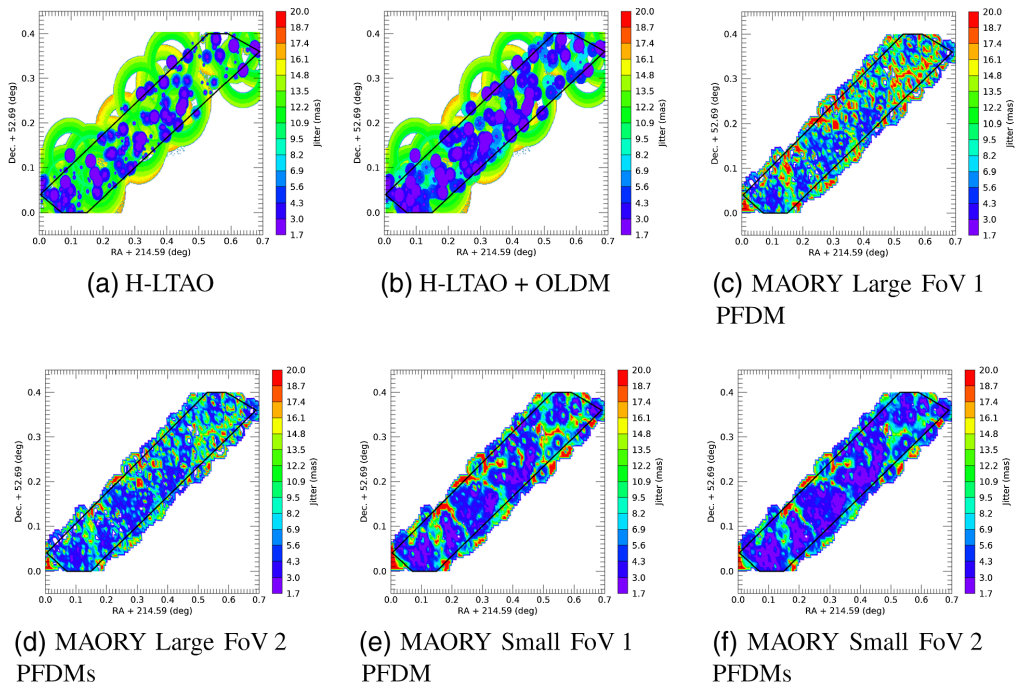

(a) H-LTAO

(b) H-LTAO + OLDM

(c) MAORY Large FoV 1 PFDM

(d) MAORY Large FoV 2 PFDMs

(e) MAORY Small FoV 1 PFDM

(f) MAORY Small FoV 2 PFDMs

Fig. 11 Jitter with H-LTAO (on axis) or with MAORY (averaged on the scientific FoV) for the EGS field. The jitter is limited to 20 mas for a better display. The black lines indicate the area used for the SC computation.

(20×20"). In this configuration, the NGSs sensors of MAORY can reach stars closer to the axis, as shown in Table 1. The performance is then averaged as indicated in Fig. 5.

It is interesting to note that MAORY, with the large MICADO FoV, never reaches the minimum jitter (i.e., the jitter at 0% SC, see for example, Fig. 19) as low as the one from H-LTAO: the
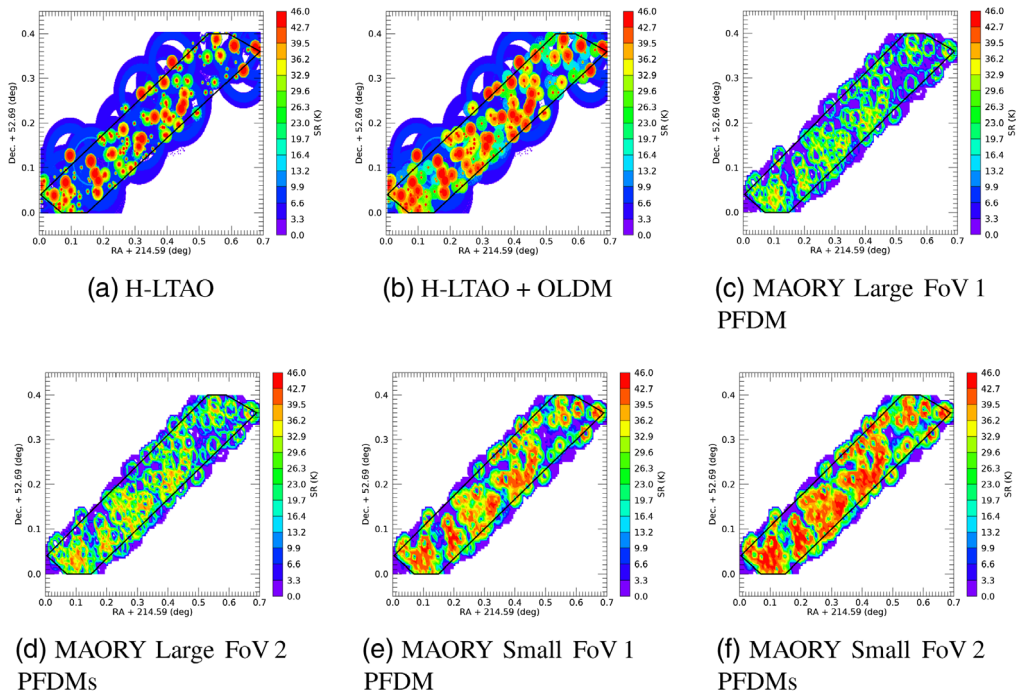
(a) H-LTAO

(b) H-LTAO + OLDM

(c) MAORY Large FoV 1 PFDM

(d) MAORY Large FoV 2 PFDMs

(e) MAORY Small FoV 1 PFDM

(f) MAORY Small FoV 2 PFDMs

Fig. 12 SR in K band with H-LTAO (on axis) or with MAORY (averaged on the scientific FoV) for the EGS field. The black lines indicate the area used for the SC computation.
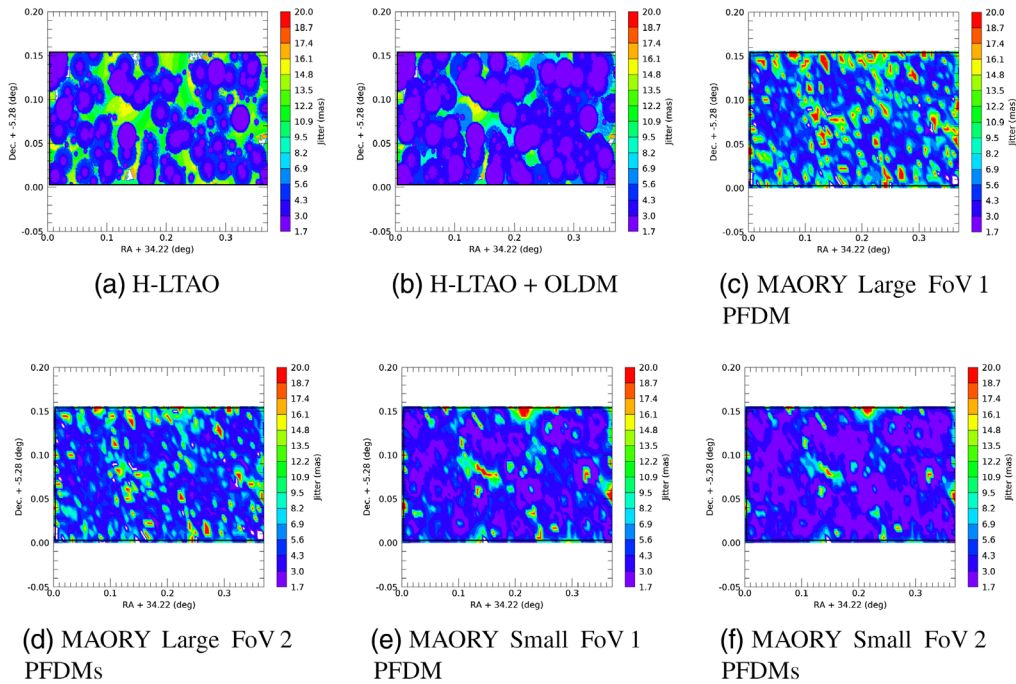

(a) H-LTAO

(b) H-LTAO + OLDM

(c) MAORY Large FoV 1 PFDM

(d) MAORY Large FoV 2 PFDMs

(e) MAORY Small FoV 1 PFDM

(f) MAORY Small FoV 2 PFDMs

Fig. 13 Jitter with H-LTAO (on axis) or with MAORY (averaged on the scientific FoV) for the UDS field. The jitter is limited to 20 mas for a better display. The black lines indicate the area used for the SC computation.

best available asterism for MAORY is not the best that the system could actually expect with an infinite number of bright stars, while the best case for H-LTAO (i.e., an on-axis bright NGS) does happen here. The ability of AO systems to deal with this type of situation is particularly interesting as we are looking at the limits of their performance in presence of only few NGSs.
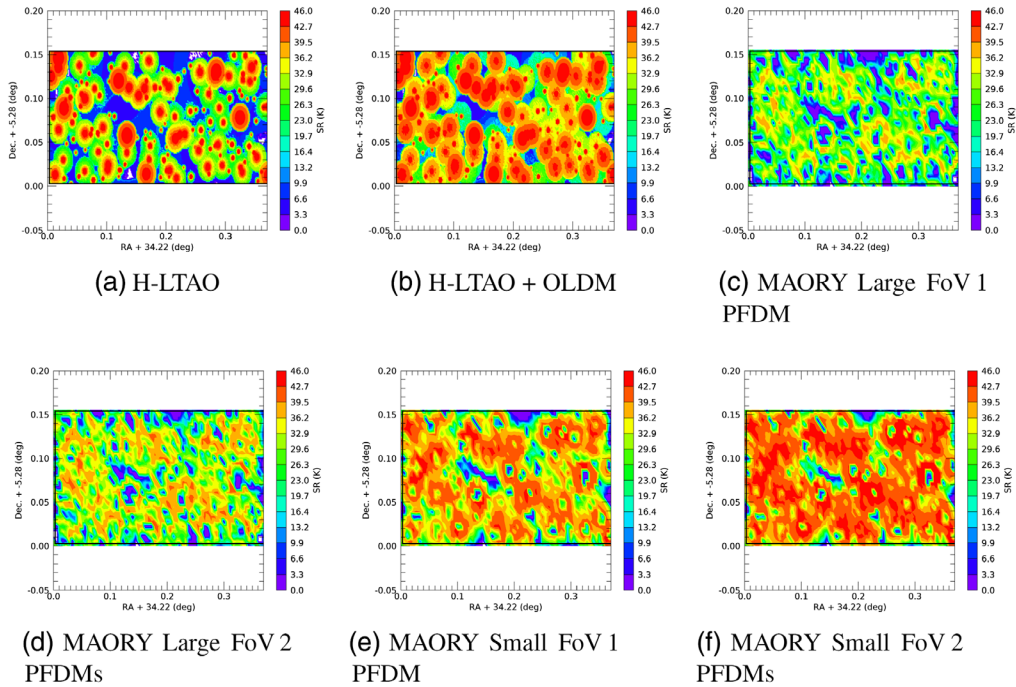
(a) H-LTAO

(b) H-LTAO + OLDM

(c) MAORY Large FoV 1 PFDM

(d) MAORY Large FoV 2 PFDMs

(e) MAORY Small FoV 1 PFDM

(f) MAORY Small FoV 2 PFDMs

Fig. 14 SR in K band with H-LTAO (on axis) or with MAORY (averaged on the scientific FoV) for the UDS field. The black lines indicate the area used for the SC computation.
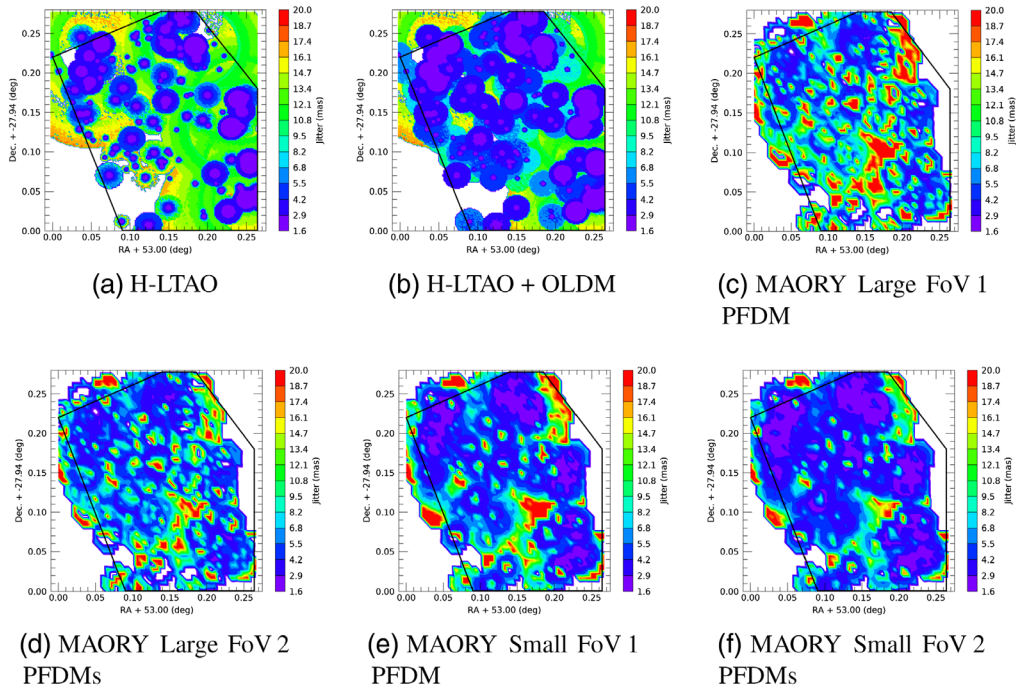

(a) H-LTAO

(b) H-LTAO + OLDM

(c) MAORY Large FoV 1 PFDM

(d) MAORY Large FoV 2 PFDMs

(e) MAORY Small FoV 1 PFDM

(f) MAORY Small FoV 2 PFDMs

Fig. 15 Jitter with H-LTAO (on axis) or with MAORY (averaged on the scientific FoV) for the GOODS-S field. The jitter is limited to 20 mas for a better display. The black lines indicate the area used for the SC computation.

The two systems also offer a similar peak performance, with a SR of about 45% in K band and a few mas of jitter. (We recall that MAORY's performance is averaged on the whole scientific FoV, hence its peak performance on axis is higher (typically a few points of SR) than the numbers written here.) The median performance is quite dependent on the field and/or the
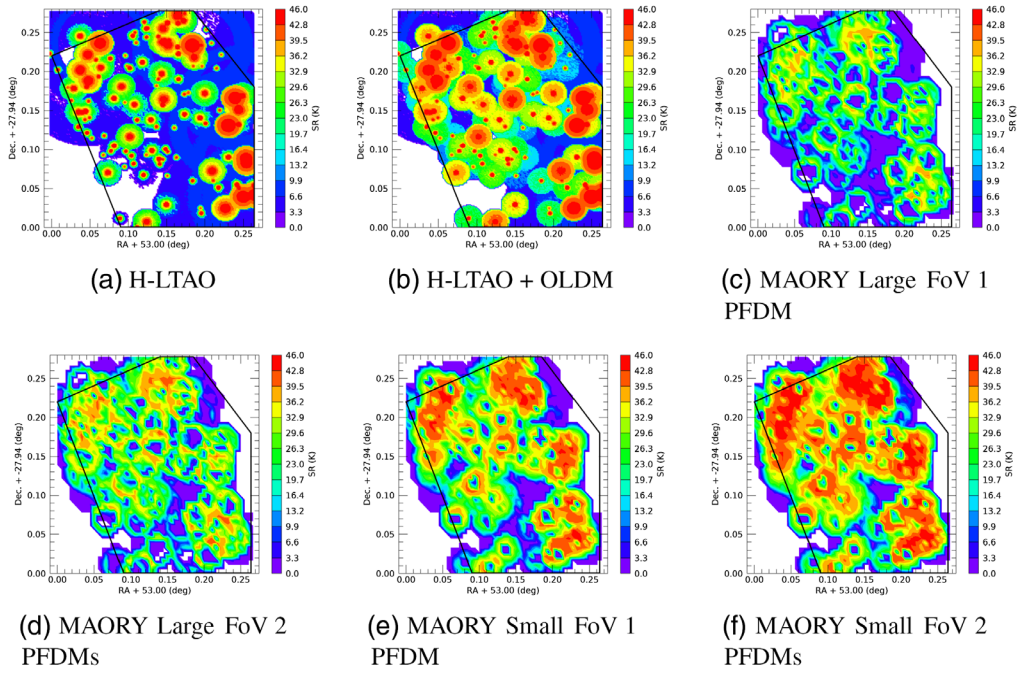
(a) H-LTAO

(b) H-LTAO + OLDM

(c) MAORY Large FoV 1 PFDM

(d) MAORY Large FoV 2 PFDMs

(e) MAORY Small FoV 1 PFDM

(f) MAORY Small FoV 2 PFDMs

Fig. 16 SR in K band with H-LTAO (on axis) or with MAORY (averaged on the scientific FoV) for the GOODS-S field. The black lines indicate the area used for the SC computation.
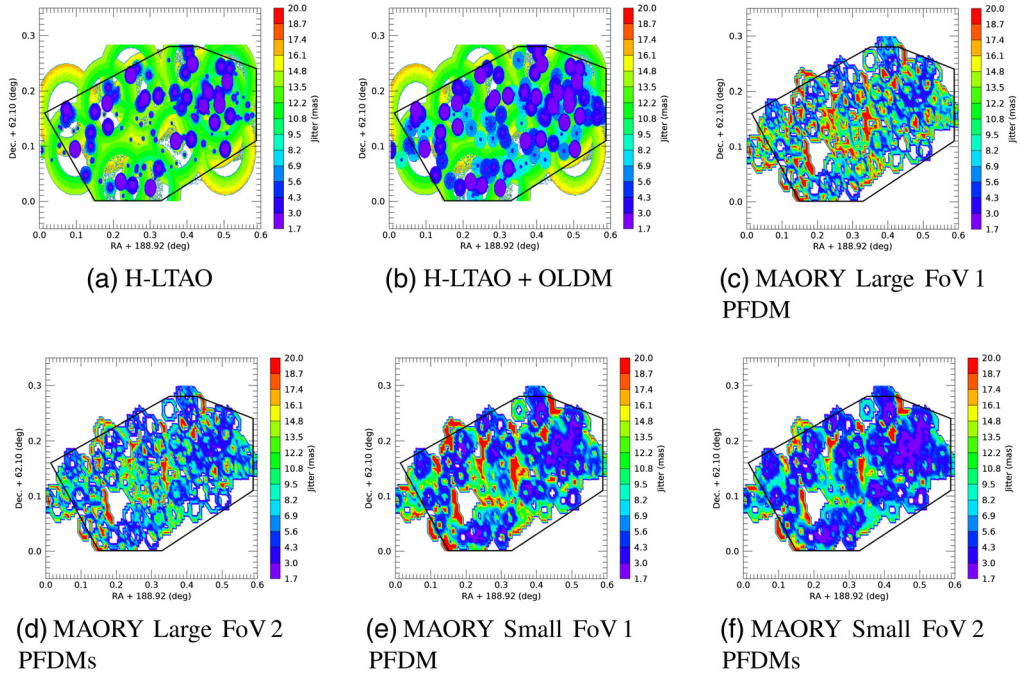

(a) H-LTAO

(b) H-LTAO + OLDM

(c) MAORY Large FoV 1 PFDM

(d) MAORY Large FoV 2 PFDMs

(e) MAORY Small FoV 1 PFDM

(f) MAORY Small FoV 2 PFDMs

Fig. 17 Jitter with H-LTAO (on axis) or with MAORY (averaged on the scientific FoV) for the GOODS-N field. The jitter is limited to 20 mas for a better display. The black lines indicate the area used for the SC computation.

configuration of the system: the median jitter is below 5 mas for the best fields (COSMOS and UDS), leading to median SRs ranging between 30% and 40%, while the median jitter in the worst field (GOODS-N) can go up to between 10 and 15 mas for the lowest-performing configurations, leading to median SRs below 10%. Better configurations (H-LTAO with the OLDM, MAORY with 2 PFDMs and/or with the small MICADO FoV) provide better robustness, with
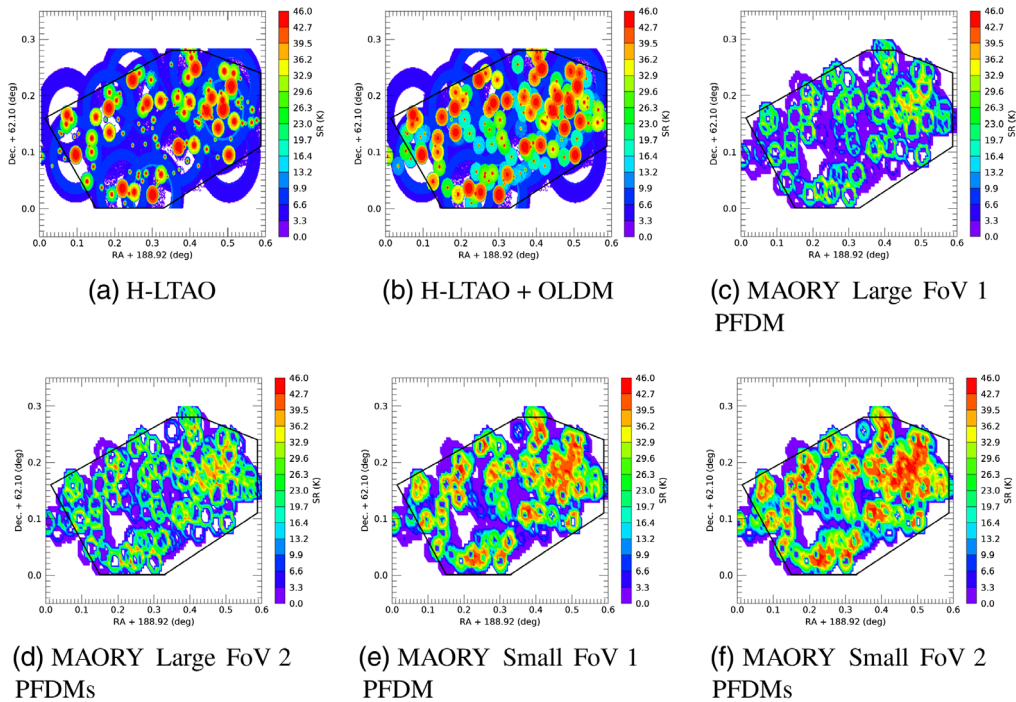
(a) H-LTAO (b) H-LTAO + OLDM (c) MAORY Large FoV 1 PFDM

(d) MAORY Large FoV 2 PFDMs (e) MAORY Small FoV 1 PFDM (f) MAORY Small FoV 2 PFDMs

Fig. 18 SR in K band with H-LTAO (on axis) or with MAORY (averaged on the scientific FoV) for the GOODS-N field. The black lines indicate the area used for the SC computation.
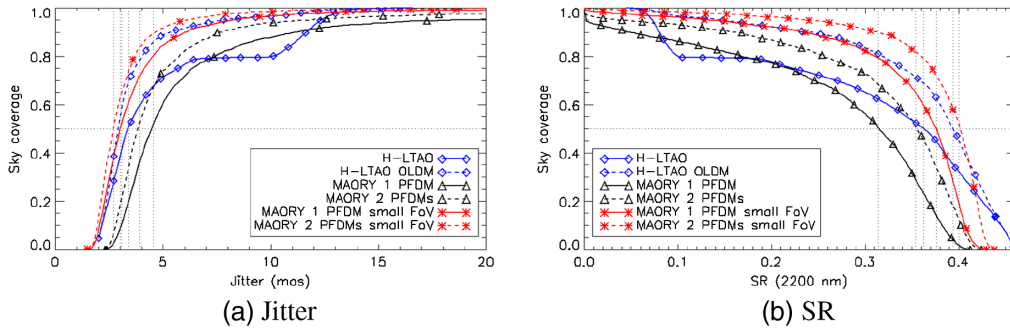

(a) Jitter (b) SR

Fig. 19 SC with H-LTAO or with MAORY for the COSMOS field. The jitter/SR is on axis for H-LTAO and averaged on a 1 arcmin diameter FoV (large FoV) or on a 20" diameter FoV (small FoV) for MAORY.
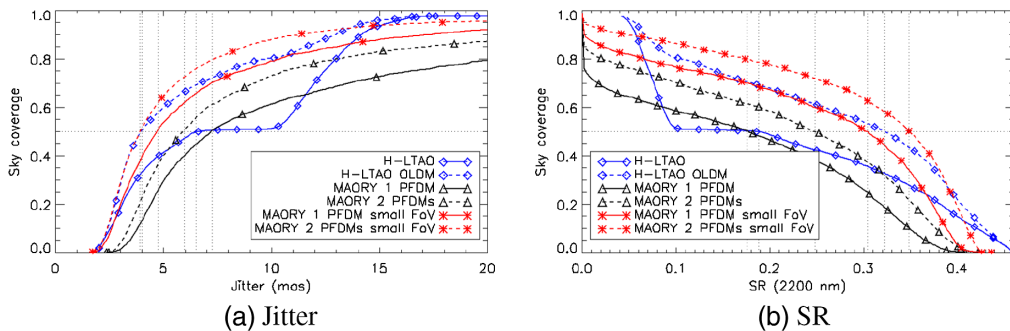

(a) Jitter (b) SR

Fig. 20 SC with H-LTAO or with MAORY for the EGS field. The jitter/SR is on axis for H-LTAO and averaged on a 1 arcmin diameter FoV (large FoV) or on a 20" diameter FoV (small FoV) for MAORY.
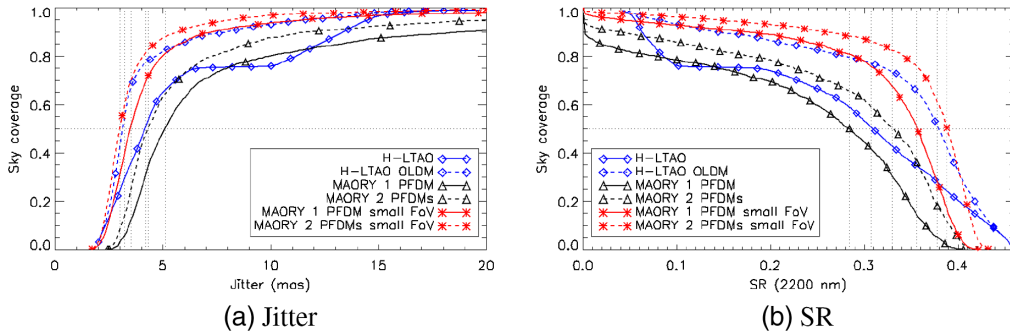
(a) Jitter (b) SR

Fig. 21 SC with H-LTAO or with MAORY for the UDS field. The jitter/SR is on axis for H-LTAO and averaged on a 1 arcmin diameter FoV (large FoV) or on a 20" diameter FoV (small FoV) for MAORY.
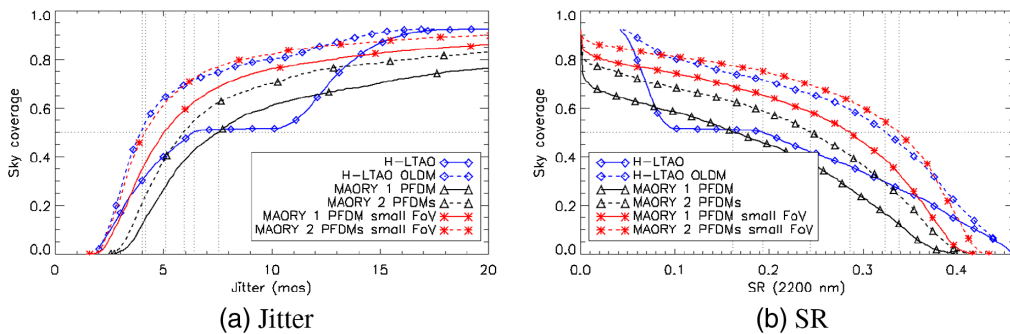

(a) Jitter (b) SR

Fig. 22 SC with H-LTAO or with MAORY for the GOODS-S field. The jitter/SR is on axis for H-LTAO and averaged on a 1 arcmin diameter FoV (large FoV) or on a 20" diameter FoV (small FoV) for MAORY.

(a) Jitter (b) SR

Fig. 23 SC with H-LTAO or with MAORY for the GOODS-N field. The jitter/SR is on axis for H-LTAO and averaged on a 1 arcmin diameter FoV (large FoV) or on a 20" diameter FoV (small FoV) for MAORY.
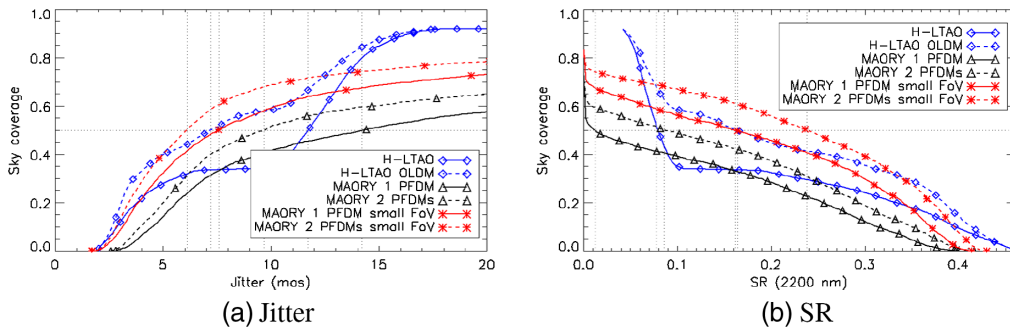
median SRs roughly ranging between 10% and 20% in the GOODS-N field. From this results, we can derive approximate equivalencies between the two systems. H-LTAO without the OLDM gives a performance that approximately is between MAORY's baseline configuration (one PFDM, large MICADO FoV) and the upgraded configuration (two PFDMs, large MICADO FoV), though it provides a better SC at both ends (low SC/high performance and high SC/low performance). With the OLDM in H-LTAO, the performance gets similar to what we can expect

Table 5 Jitter/SR reached by the considered systems for different levels of SC in the COSMOS field.

Instrument/configuration	Jitter (mas)			SR (2200 nm)		
	25% SC	50% SC	75% SC	25% SC	50% SC	75% SC
H-LTAO	2.6	3.4	5.7	0.41	0.36	0.22
H-LTAO OLDM	2.5	3	3.7	0.42	0.39	0.34
MAORY 1 PFDM	3.6	4.6	6.4	0.36	0.31	0.22
MAORY 2 PFDMs	3.2	3.9	5.2	0.39	0.35	0.29
MAORY 1 PFDM small FoV	2.4	3.1	4.2	0.42	0.4	0.34
MAORY 2 PFDMs small FoV	2.3	2.7	3.5	0.44	0.42	0.38

Table 6 Jitter/SR reached by the considered systems for different levels of SC in the EGS field.

Instrument/configuration	Jitter (mas)			SR (2200 nm)		
	25% SC	50% SC	75% SC	25% SC	50% SC	75% SC
H-LTAO	3.4	6.5	12.5	0.36	0.19	0.07
H-LTAO OLDM	3	4	8	0.39	0.32	0.14
MAORY 1 PFDM	4.8	7.3	16.4	0.30	0.18	0
MAORY 2 PFDMs	4.2	6	10.6	0.34	0.25	0.06
MAORY 1 PFDM small FoV	3.2	4.7	8.6	0.39	0.31	0.12
MAORY 2 PFDMs small FoV	2.9	3.9	6.4	0.41	0.36	0.23

Table 7 Jitter/SR reached by the considered systems for different levels of SC in the UDS field.

Instrument/configuration	Jitter (mas)			SR (2200 nm)		
	25% SC	50% SC	75% SC	25% SC	50% SC	75% SC
H-LTAO	3.1	4.2	6.5	0.39	0.31	0.19
H-LTAO OLDM	2.7	3.2	4	0.41	0.38	0.32
MAORY 1 PFDM	4	5.1	8	0.34	0.28	0.14
MAORY 2 PFDMs	3.5	4.3	6.3	0.37	0.33	0.23
MAORY 1 PFDM small FoV	2.9	3.5	4.5	0.40	0.38	0.32
MAORY 2 PFDMs small FoV	2.6	3	3.8	0.42	0.40	0.37

Table 8 Jitter/SR reached by the considered systems for different levels of SC in the GOODS-S field.

	Jitter (mas)			SR (2200 nm)		
Instrument/configuration	25% SC	50% SC	75% SC	25% SC	50% SC	75% SC
H-LTAO	3.6	6.4	13.2	0.35	0.19	0.06
H-LTAO OLDM	3	4	7.7	0.39	0.32	0.15
MAORY 1 PFDM	4.9	7.5	18.1	0.29	0.16	0
MAORY 2 PFDMs	4.2	5.9	11.8	0.33	0.24	0.04
MAORY 1 PFDM small FoV	3.6	5.1	9.4	0.37	0.30	0.09
MAORY 2 PFDMs small FoV	3.1	4.2	6.9	0.40	0.35	0.20

Table 9 Jitter/SR reached by the considered systems for different levels of SC in the GOODS-N field.

	Jitter (mas)			SR (2200 nm)		
Instrument/configuration	25% SC	50% SC	75% SC	25% SC	50% SC	75% SC
H-LTAO	4.5	11.7	13.7	0.29	0.08	0.06
H-LTAO OLDM	3.3	7.2	12.8	0.37	0.16	0.07
MAORY 1 PFDM	6.3	14.2	119	0.22	0.01	0
MAORY 2 PFDMs	5.5	9.7	63	0.27	0.09	0
MAORY 1 PFDM small FoV	4.3	7.6	23.1	0.34	0.17	0
MAORY 2 PFDMs small FoV	3.8	6.1	15.1	0.37	0.24	0.01

with the small MICADO FoV for MAORY. In that case, the performance is closer to MAORY with two PFDMs at both ends and to MAORY with one PFDM in the knee of the SC curve.

5 Discussion

The jitter and SR maps present a recurrent pattern: the performance of MAORY is best around the areas where the performance of H-LTAO is best. Indeed, H-LTAO needs only one NGS that can be close to the optical axis of the telescope, whereas MAORY makes use of up to three NGSs, that need to be at a minimum distance of 49" (large MICADO FoV) or 24" (small MICADO FoV) to avoid vignetting the scientific FoV. This means that the SR delivered by H-LTAO peaks for pointings close to a bright star and drops quickly when going away from this star, while the SR delivered by MAORY reaches a maximum when the NGSs are not within the science FoV. Besides, we note that the two systems reach similar levels of jitter and SR on the bright end. They are thus complementary in terms of SC, meaning that the overall SC of ESO's ELT is extremely good for applications that are common to the two systems.

The H-LTAO performance (without OLDM) shows a sort of bimodal distribution, with a first plateau of performance up to a jitter limit around 10 mas, and then a second increase of SC. This behavior is explained by the transition between the sequential and cascade modes, where in the first case we use the closest and brightest stars to perform most of the jitter control, while in the second case the telescope guide probe is mostly controlling the jitter. The transition between

these two regimes will highly depend on the telescope guiding performance and could potentially be optimized. Note that if NGSs fainter than $H = 19$ were considered, the plateau would appear at better performance. On the other hand, the gain brought by the OLDM can also improve the performance in this exact regime, by providing a better residual jitter for far and faint NGS. This translates into a better SR over a wider area of these cosmological field. It is however important to mention that the OLDM performance gain presented in this study must be seen as the optimistic upper limit. Indeed, the OLDM off-axis performance has been evaluated in an ideal case where only fitting and off-axis tomography were considered in the error budget. Taking into account a more realistic error budget for the OLDM off-axis performance, including for instance the open loop control, DM creep, calibration issues would reduce the expected off-axis Strehl, degrade the expected noise propagation, and eventually increase the residual jitter. The final and realistic performance to be expected with OLDM certainly lies in between the two performance plots shown in this study.

For MAORY, the second PFDM also improves the overall SC, but the most significant gain in performance is when considering the small MICADO FoV instead of the large one: it surpasses by far the gain provided by the third DM. This is mostly due to the additional area given to the technical FoV, which allows the selection of more stars in general and especially ones closer to the optical axis, which provide a better tomography. It would thus be preferable for an MCAO system to get rid of the central obscuration of the technical FoV as much as possible, for example, by sensing the NGSs at a wavelength not used by the science path. Though this solution might put difficult constraints on the design, it can be straightforwardly applied in a system such as MAVIS (MCAO-assisted visible imager and spectrograph),[27] which will do science in the visible.

6 Conclusion

The SC of an instrument is a key feature for observations: having a good resolution on only a few objects strongly limits the studies that can be performed by the astronomers. It is thus important to make sure that future AO systems, such as MAORY and H-LTAO for ESO's ELT, will provide a satisfying SC.

In this paper, we presented the SC assessment methods of MAORY and HARMONI. Though there are some differences between the two approaches, the general method is the same and could be applied for any other tomographic AO system: evaluate the HO part of the wavefront error, which is independent from the NGS asterism, then compute the statistics of the LO part using a series of randomly generated fields. The LO residuals are the sum of a purely geometric tomographic error that only depends on the NGS asterism geometry; the noise propagation through the tomographic reconstruction that depends on the WFS sensitivity, the NGSs' magnitudes and the correction level in the technical FoV; and the residual vibrations due to windshake. Other terms of wavefront error that are independent from either the NGS asterism or the whole AO system itself can be independently added afterward.

We have then evaluated the performance of both MAORY and H-LTAO in already known cosmological fields. These results can be taken as an indication of the image quality on MICADO and HARMONI in sky areas that are poor in bright stars, hence where the AO is pushed to its limits. We have confirmed that the use of an OLDM can increase the SC of an LTAO system. Likewise, the addition of a second post-focal DM for MAORY provides a significant gain in performance. We also noted that reducing the central obscuration of the technical FoV of MAORY, which happens when using MICADO's small FoV, leads to a much better performance as well. This encourages the choice of an NGS sensing wavelength not used by the science for MCAO systems, though it might be difficult in practice. Finally, we have shown that, if applications concur, the SC provided by the two systems can be complementary. The overall SC of the telescope is thus greatly improved.

7 Appendix A: Computation of Tomographic Error

The goal of this appendix is to compute the LO residual in a direction α due to the tomographic reconstruction error. We assume that we will perform a split tomography, meaning that the HO

(modes from focus, sensed with the LGSs) and LO modes (TT, sensed with the NGSs) will be estimated separately. We can thus assess the tomographic error using the NGSs only. We can write the estimation of the LO modes in the direction α as

$$\hat{a} = R(s + n), \tag{8}$$

where $\hat{a}$ is the estimate of a, the vector of LO modes coefficients in the direction α; s is the vector grouping all the measured LO modes coefficients for all NGSs; n is the noise on these measurements and R is the reconstructor. We define here the reconstructor as

$$R = P_\alpha W, \tag{9}$$

where P_α is the projection in the direction α and W is the tomographic reconstructor, computed with two layers (TT on ground layer and focus/astigmatism on altitude layer). The covariance matrix of the LO modes in the direction α can then be expressed as (assuming the noise is not correlated with a nor s):

$$\langle (a - \hat{a})(a - \hat{a})^t \rangle = C_{aa} - C_{as}R^t - RC_{as}^t + RC_{ss}R^t + RC_{nn}R^t, \tag{10}$$

where $C_{xy} = \langle xy^t \rangle$ is the covariance between x and y. The equation to compute these covariance matrices for Zernike modes is given in Appendix B. In this paper, the noise covariance matrix C_{nn} is considered diagonal, with a uniformly distributed noise on the two LO modes (example for a three-NGS asterism with MAORY):

$$C_{nn} = \begin{bmatrix} \sigma_1^2/2 & 0 & \cdots & \cdots & \cdots & 0 \\ 0 & \sigma_1^2/2 & 0 & \cdots & \cdots & \vdots \\ \vdots & 0 & \sigma_2^2/2 & 0 & \cdots & \vdots \\ \vdots & \cdots & 0 & \sigma_2^2/2 & 0 & \vdots \\ \vdots & \cdots & \cdots & 0 & \sigma_3^2/2 & 0 \\ 0 & \cdots & \cdots & \cdots & 0 & \sigma_3^2/2 \end{bmatrix}, \tag{11}$$

where σ_k^2 is the total noise variance on the k'th NGS.

We can finally define the tomographic error as

$$\sigma_{\text{tomo,tot}} = \sqrt{\sigma_{\text{tomo,0}}^2 + \sigma_{\text{tomo},n}^2}, \tag{12}$$

with

$$\sigma_{\text{tomo,0}}^2 = C_{aa} - C_{as}R^t - RC_{as}^t + RC_{ss}R^t, \tag{13}$$

the pure tomographic error and

$$\sigma_{\text{tomo},n}^2 = RC_{nn}R^t, \tag{14}$$

the tomographic noise error.

8 Appendix B: Computation of Zernike Modes Covariances

The covariance between two Zernike mode coefficients a_j and a_k (in Noll's definition[28]) in the direction of two different stars at coordinates $\vec{\theta_1}$ and $\vec{\theta_2}$ is, for a telescope of radius R:[29]

$$\langle a_j(\vec{\theta}_1)a_k(\vec{\theta}_2)\rangle = (-1)^{m_k}\sqrt{(n_j+1)(n_k+1)}i^{n_j+n_k}2^{1-0.5(\delta_{0m_j}+\delta_{0m_k})}$$

$$\times \int dh \frac{1}{\pi R^2\left(1-\frac{h}{z_1}\right)\left(1-\frac{h}{z_2}\right)}$$

$$\times \int_0^\infty \frac{df}{f}W_\varphi(h,f)J_{n_j+1}\left(2\pi f R\left(1-\frac{h}{z_1}\right)\right)J_{n_k+1}\left(2\pi f R\left(1-\frac{h}{z_2}\right)\right)$$

$$\times \left\{\cos((m_j+m_k)\arg(\vec{\theta}_1-\vec{\theta}_2)+\frac{\pi}{4}((1-\delta_{0m_j})((-1)^j-1)+(1-\delta_{0m_k})((-1)^k-1)))\right.$$

$$\times i^{3(m_j+m_k)}J_{m_j+m_k}(2\pi fh|\vec{\theta}_1-\vec{\theta}_2|)+\cos((m_j-m_k)\arg(\vec{\theta}_1-\vec{\theta}_2)$$

$$+\frac{\pi}{4}((1-\delta_{0m_j})((-1)^j-1)-(1-\delta_{0m_k})((-1)^k-1)))$$

$$\left.\times i^{3|m_j-m_k|}J_{|m_j-m_k|}(2\pi fh|\vec{\theta}_1-\vec{\theta}_2|)\right\}, \tag{15}$$

where n_j and m_j are the radial and azimuthal orders of the j'th polynomial, δ_{0x} is the Kronecker delta between 0 and x, h is the layer altitude, z_1 and z_2 are the altitudes of the two stars (= infinity for NGSs), $J_n(x)$ is the Bessel function of first kind of order n, f is the spatial frequency, and $W_\varphi(h,f)$ is the turbulent phase PSD for the layer at altitude h. The turbulent PSD used in this paper is the one defined by Von-Karman:

$$W_\varphi(h,f) = 0.023r_0(h)^{-\frac{5}{3}}\left(f^2+\frac{1}{L_0^2}\right)^{-\frac{11}{6}}, \tag{16}$$

where r_0 is the Fried parameter and L_0 is the outer scale (= 25 m throughout the paper).

9 Appendix C: Model Validation

For MAORY, the LO residual (without windshake) in one direction of the scientific FoV is computed from the noise error interpolation described in Sec. 3.2.4 and the tomographic error described in Sec. 3.2.3. This residual can be verified with E2E simulations. We performed a sanity check of the residual on axis with the asterisms used for the noise interpolation on one hand (Fig. 24) and random three-NGS asterisms on the other hand (Fig. 25). The random asterisms have distance and magnitude values chosen from the ones of Sec. 3.2.4 and the angle values are limited to steps of 30 deg. The pick-up mirror collisions were not considered, so two stars could fall at the same place, thus some of the asterisms are equivalent to two-NGS asterisms.

We have a good match between the real residual and the estimated one. On the equilateral asterisms (Fig. 24), we see that we might overestimate a bit the error at high flux and underestimate it at low flux, but we always fall within the error bars, which we consider a sufficient
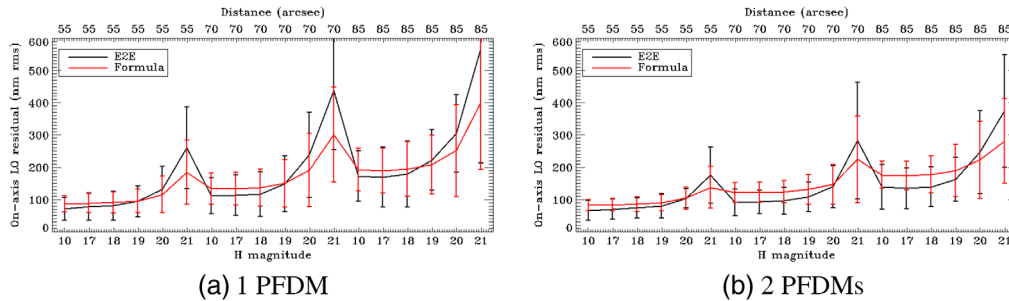

(a) 1 PFDM

(b) 2 PFDMs

Fig. 24 Comparison of the LO residual on axis from the E2E simulations and from the formula. (a) With one PFDM and (b) with two PFDMs. All asterisms are equilateral triangles, with all the stars at the same distance and the same magnitude (indicated on the x axis).
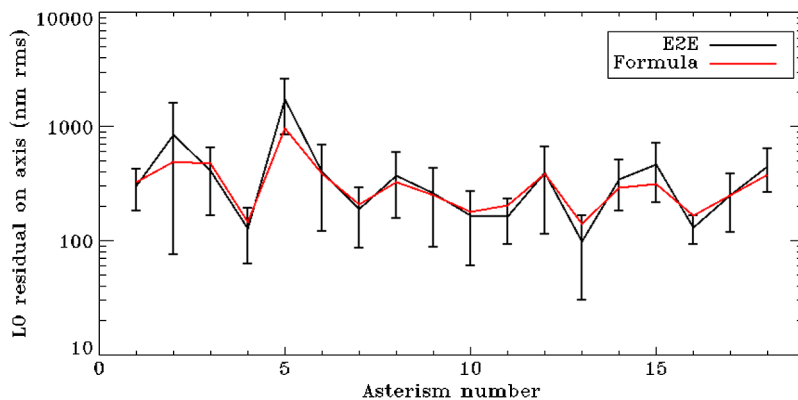
Fig. 25 Comparison of the LO residual on axis from the E2E simulations and from the formula, for 18 random asterisms and two DMs.
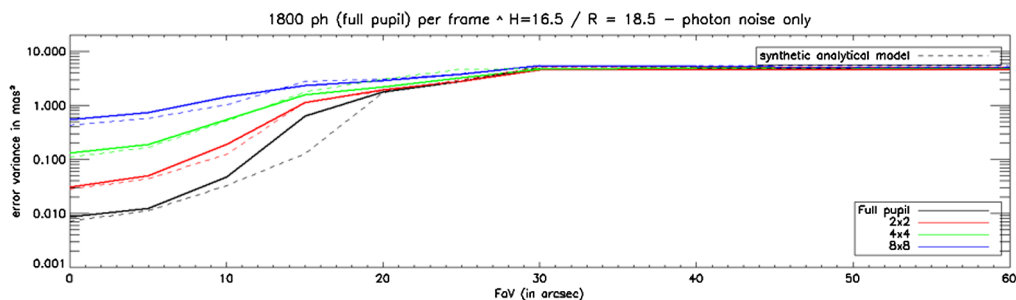

Fig. 26 Evolution of the noise variance (in mas^2) as a function of the FoV position. Solid line = simulation, dotted line = analytical expression in the good SR regime, dashed-line = FWHM regime.

level of precision for this analysis. Looking at random asterisms (Fig. 25) that represent more significantly what we can expect in the SC analysis, the match is satisfying as well. We thus consider that our model is valid.

In the case of H-LTAO, a comparison between the E2E simulation and the modified analytical model is shown in Fig. 26.

Note that we checked that similar good match between the analytical model and the E2E simulations were valid for other fluxes levels. We also checked the good behavior of the model when RON is added.

Acknowledgments

References

1. M. Lyubenova, et al., "European extremely large telescope ESO," https://elt.eso.org/credits/ (accessed 2010-09-30).

2. P. Ciliegi et al., "MAORY for ELT: preliminary design overview," *Proc. SPIE* **10703**, 1070311 (2018).

3. R. Davies et al., "MICADO: first-light imager for the E-ELT," *Proc. SPIE* **9908**, 99081Z (2016).

4. N. A. Thatte et al., "The E-ELT first light spectrograph HARMONI: capabilities and modes," *Proc. SPIE* **9908**, 99081X (2016).

5. B. Neichel et al., "The adaptive optics modes for HARMONI: from classical to laser assisted tomographic AO," *Proc. SPIE* **9909**, 990909 (2016).

6. B. R. Brandl et al., "Status of the mid-IR ELT imager and spectrograph (METIS)," *Proc. SPIE* **10702**, 107021U (2018).

7. F. Vidal et al., "Analysis the MICADO-MAORY SCAO performance," in *Proc. AO4ELT6 Conf.*, p. 251 (2019).

8. N. Schwartz et al., "Design of the HARMONI Pyramid WFS module," arXiv:2003.07228 (2020).

9. T. Bertram et al., "Single conjugate adaptive optics for METIS," *Proc. SPIE* **10703**, 1070314 (2018).

10. B. L. Ellerbroek and D. W. Tyler, "Adaptive optics sky coverage calculations for the Gemini-North telescope," *Publ. Astron. Soc. Pac.* **110**, 165–185 (1998).

11. M. Le Louarn et al., "Simulations of adaptive optics systems for the E-ELT," *Proc. SPIE* **8447**, 84475D (2012).

12. M. Tallon and R. Foy, "Adaptive telescope with laser probe: isoplanatism and cone effect," *Astron. Astrophys.* **235**, 549–557 (1990).

13. B. L. Ellerbroek and F. Rigaut, "Methods for correcting tilt anisoplanatism in laser-guide-star-based multiconjugate adaptive optics," *J. Opt. Soc. Am. A* **18**, 2539–2547 (2001).

14. T. Fusco et al., "Optimal wave-front reconstruction strategies for multiconjugate adaptive optics," *J. Opt. Soc. Am. A* **18**, 2527–2538 (2001).

15. R. Foy and A. Labeyrie, "Feasibility of adaptive telescope with laser probe," *Astron. Astrophys.* **152**, L29–L31 (1985).

16. T. Fusco et al., "Sky coverage estimation for multiconjugate adaptive optics systems: strategies and results," *Mon. Not. Natl. R. Astron. Soc.* **370**, 174–184 (2006).

17. D. Andersen et al., "Predicted sky coverage for the TMT MCAO system NFIRAOS," in *Second Int. Conf. Adapt. Opt. for Extrem. Large Telesc.*, p. 18, http://ao4elt2.lesia.obspm.fr (2011).

18. I. Damjanov et al., "Extragalactic fields optimized for adaptive optics," *Publ. Astron. Soc. Pac.* **123**, 348 (2011).

19. A. Robin and M. Creze, "Stellar populations in the Milky way: a synthetic model," *Astron. Astrophys.* **157**, 71–90 (1986).

20. N. A. Grogin et al., "CANDELS: the cosmic assembly near-infrared deep extragalactic legacy survey," *Astrophys. J. Suppl. Ser.* **197**, 35 (2011).

21. A. M. Koekemoer et al., "CANDELS: the cosmic assembly near-infrared deep extragalactic legacy survey—the Hubble space telescope observations, imaging data products, and mosaics," *Astrophys. J. Suppl. Ser.* **197**, 36 (2011).

22. J. Kolb et al., "Relevant atmospheric parameters for E-ELT AO analysis and simulations," Internal document ESO-258292, version 2 (2015).

23. T. Pfrommer and P. Hickson, "High-resolution lidar observations of mesospheric sodium and implications for adaptive optics," *J. Opt. Soc. Am. A* **27**, A97 (2010).

24. F. Rigaut and E. Gendron, "Laser guide star in adaptive optics: the tilt determination problem," *Astron. Astrophys.* **261**, 677–684 (1992).

25. "Data package for ELT simulations," ESO-315732.

26. M. Nicolle et al., "Improvement of Shack–Hartmann wave-front sensor measurement for extreme adaptive optics," *Opt. Lett.* **29**(23), 2743–2745 (2004).

27. F. Rigaut et al., "MAVIS conceptual design," *Proc. SPIE* **11447**, 114471R (2020).

28. R. J. Noll, "Zernike polynomials and atmospheric turbulence," *Opt. Soc. Am.* **66**, 207–211 (1976).
29. M. R. Whiteley, M. C. Roggemann, and B. M. Welsh, "Temporal properties of the Zernike expansion coefficients of turbulence-induced phase aberrations for aperture and source motion," *J. Opt. Soc. Am. A* **15**, 993–1005 (1998).

Cédric Plantet received his PhD from the Paris Observatory University in 2014. His work was focused on focal-plane wavefront sensing with the Linearized Focal-plane Technique (LIFT). After a first post-doc at Onera and LAM on infrared wavefront sensing, he joined INAF-Osservatorio Astrofisico di Arcetri in 2016 to work on MAORY and then other Adaptive Optics projects such as MAVIS. His current work is mostly focused on semianalytical simulations for adaptive optics and natural guide star wavefront sensing.

Benoît Neichel received his PhD from the Paris Observatory University in 2008. His work was focused on integral field spectroscopy (IFS) observations of distant galaxies and wide field adaptive optics (WFAO) systems for extragalactic observations on extremely large telescopes (ELTs). He then worked as an instrument scientist for the Gemini GeMS instrument, which was the first WFAO system implemented on an 8 m telescope and offered to the astronomical community. In 2013, he joined Laboratoire d'Astrophysique de Marseille (LAM) as a full-time scientist. He is now the deputy-PI for HARMONI the first light IFS for the European ELT, and he is leading the research and development department of LAM.

Biographies of the other authors are not available.